Enhanced Intrinsic Skin Aging in Nephropathic Cystinosis Assessed by High-Definition Optical Coherence Tomography

Journal of Investigative Dermatology (2019) **139,** 2242–2245; doi:10.1016/j.jid.2019.03.1153

TO THE EDITOR

Cystinosis is a rare autosomal recessive lysosomal storage disorder, caused by the mutations in the *CTNS* gene, which leads to the dysfunction of the cystine transporter cystinosin. Although nephropathic cystinosis is characterized by kidney disease, which is the first and the most severe feature of this disorder, it is a multisystem disease in which several clinical signs suggest the skin to be a part of the phenotype (Elmonem et al., 2016). This includes a fair complexion of the hair and skin, mainly in Caucasian patients, and progressive coarse facial features and variable degrees of atrophy and telangiectasia in adult patients (Guillet et al.,1998; Figure 1d). Considering that cystine crystal accumulation in dermal macrophages and fibroblasts and the impairment of melanogenesis have only partially substantiated the dermatological involvement in cystinosis so far, a systematic quantitative study using the most advanced noninvasive imaging technology is warranted (Chiaverini et al., 2012, 2013). High-definition optical coherence tomography (HD-OCT) is a novel, noninvasive optical imaging technique, offering advantages over in vivo reflectance confocal microscopy, such as real-time visualization at higher penetration depths (up to 570 μm), fast image acquisition, and three-dimensional reconstruction capabilities, while keeping the resolution at the cellular level (Boone et al., 2012). HD-OCT allows a deep insight into the epidermal and dermal ultrastructures. Moreover, the assessment of the tissue optical characteristics of the epidermis and papillary dermis using HD-OCT has shown to be of significant value in the diagnosis of several skin disorders (Boone et al., 2015, 2016a, 2016b). We hypothesized that in cystinosis, the dermal ultrastructure might be altered, and the tissue optical characteristics of the dermis might be affected. Hence, we aimed to identify the distinctive cutaneous features of nephropathic cystinosis by means of HD-OCT and explore its relationship with clinical disease severity. In a multicentric, cross-sectional, case-matched, international control study, a cohort of 18 patients of all ages who were diagnosed with nephropathic cystinosis (11 patients prior to kidney transplantation [KTx]) and 54 age- and sex-matched controls were recruited (see Supplementary Figure S1 and Supplementary Table S1 online). The study was approved by the Ethics Committee (Ethische Commissie Onderzoek UZ/KU Leuven number s55514; Centrum Mensgebonden Onderzoek Arnhem-Nijmegen, number 2015-2117, NL5544909115), and written informed consents were obtained from all participants; the patient depicted in Figure 1 (panel b) has provided written consent for the publication of the photographic image. The research was conducted in accordance with the Declaration of Helsinki, the principles of Good Clinical Practice, and all applicable legislations. All subjects had three HD-OCT images of the skin taken randomly within the distal third of the ventral side of the right upper arm. All of the images were taken with the same HD-OCT device (SkinTell, Agfa Healthcare, Mortsel, Belgium) and met specific requirements regarding the site of imaging (Figure 1a). Within each of the three images taken from each subject and based on predefined criteria, three regions of interest were assigned per HD-OCT image for further analysis using specialized software (Analyze 3D/Analyze BCC, version V08; SkinTell Viewer, version 24, Agfa Healthcare) (Figure 1a and see Supplementary Table S2, S3 online). In two adult KTx patients with cystinosis, reflectance confocal microscopy and HD-OCT imaging were performed at the same location of two punch skin biopsies, at the distal third of the ventral side of the right upper arm (see Supplementary Figure S2 online). Upon validation of our methodology of HD-OCT image analysis using the OCT signal versus image depth plot adapted from Boone et al. (2016a, 2016b) (see Supplementary Tables S2–S4 online), a significant reduction in epidermal ($P = 0.0074$) and papillary dermis ($P = 0.0062$) thickness was seen in patients of all ages who were diagnosed with cystinosis compared with their age- and sex-matched controls (see Supplementary Figure S1 and Supplementary Table S5 online). This epidermal ($P = 0.0095$) and papillary dermis ($P = 0.0305$) thinning was already present in non-KTx adolescent and young adult patients (Figure 1f, g, and see Supplementary Table S6 online). Thus, we exclude the possible confounding of steroid treatment in KTx recipients, while demonstrating, in a quantitative manner, the presence of a skin phenotype that points to enhanced intrinsic skin aging in cystinosis (Moloney et al., 2005; Schoepe et al., 2006). As the pathophysiology of cystinosis shares similar features associated with cellular senescence as in intrinsic skin aging, including enhanced apoptosis and impaired autophagic flux resulting in mitochondrial dysfunction and increased generation of reactive oxygen species, it is likely that these mechanisms underlie the skin phenotype (Bellomo et al., 2018; Cherqui and Courtoy, 2017; Jenkins, 2002; Levtchenko et al., 2005; Luciani et al., 2018). To explore its clinical

Abbreviations: HD-OCT, high-definition optical coherence tomography; KTx, kidney transplantation

Accepted manuscript published online 22 April 2019; corrected proof published online 27 June 2019

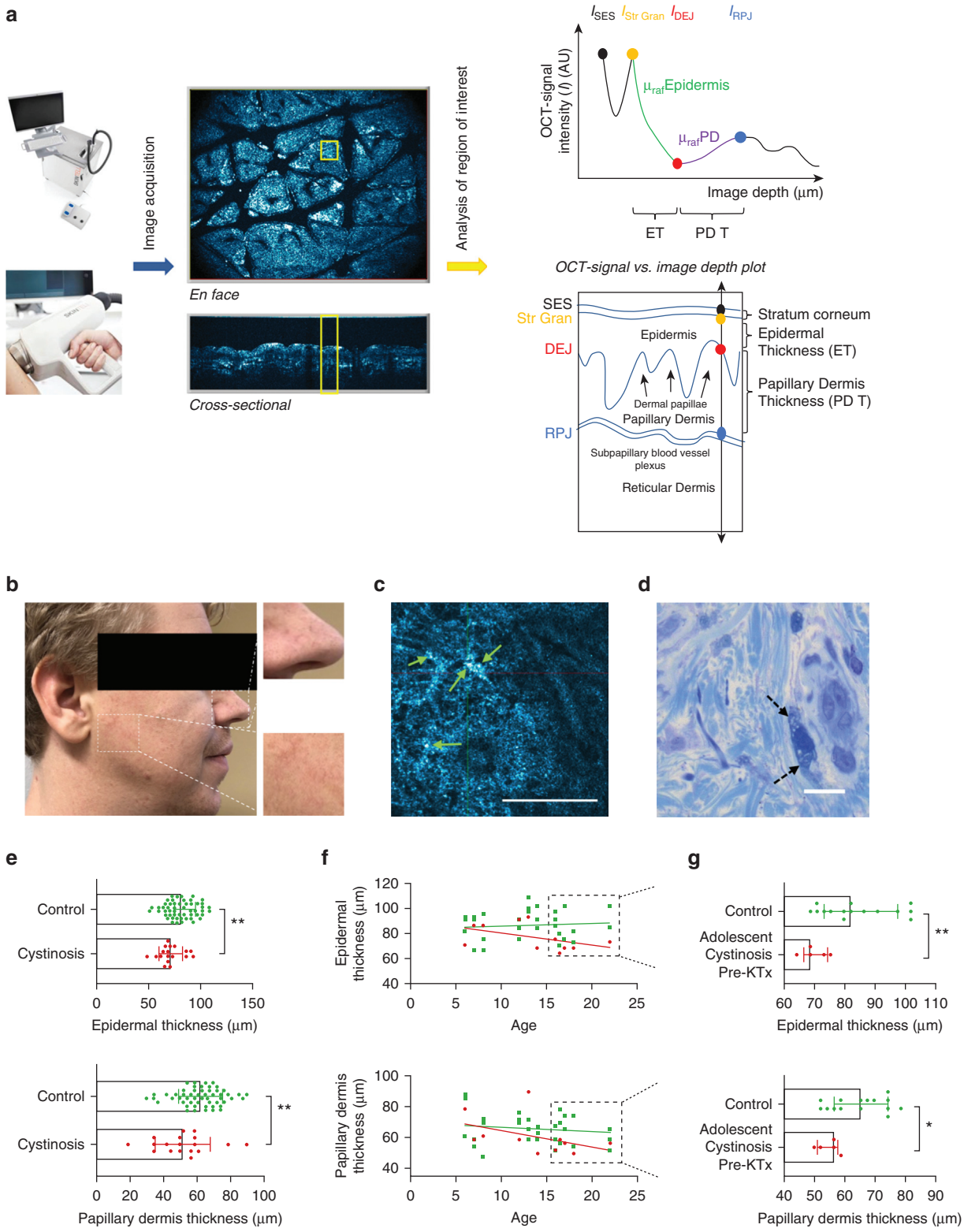

Figure 1. Epidermal and papillary dermis thinning is present in non–kidney-transplanted patients with cystinosis in adolescent and young adult age group as assessed by HD-OCT. (**a**) HD-OCT image acquisition analysis workflow. In each of the three HD-OCT images acquired, three regions of interest (yellow box) are assigned for analysis (nine observations per parameter per subject). The OCT signal versus the image depth plot is generated for each region of interest, and specific hallmarks corresponding to the anatomical substrates are assigned, yielding the parameters studied (see Supplementary Table S2 and S3 online). Photographs of the SkinTell device were a courtesy of Agfa Healthcare; reproduced with permission. (**b**) Cutaneous manifestations in a patient with cystinosis, including course facial features and telangiectasia. The patient depicted has provided written consent for the publication of the photographic image. (**c**) Correlation of HD-OCT skin image in a patient with cystinosis showing several small intensely bright deposits (green arrows; scale bar = 1000 µm) and (**d**) its corresponding histologic substrate (toluidine blue staining) showing cystine crystal depositions (dashed line; scale bar = 10 µm). (**e**–**g**) Cross-sectional analysis of epidermal and papillary dermis thickness in patients with cystinosis of all ages (d), non-KTx (e), and non-KTx adolescent and young adult patients (f)

Table 1. Significant Thinning of the Epidermis Predicts the Presence of Extrarenal Complications in Non–Kidney-Transplanted Patients with Cystinosis Harboring the Common Homozygous 57 kb Deletion of *CTNS*

Patient	Age[1]	Genetic Background	Epidermis Thinning (SD)	Extrarenal Complications[2] (n)
2	6.5	Hom 57 kb del	0	1
7	16.0	Hom 57 kb del	−2	1
9	16.9	Hom 57 kb del	0	0
10	18.0	Hom 57 kb del	−2	2
11	22.2	Hom 57 kb del	−2	1

Thinning of the epidermis is expressed as the number of standard deviations below the average of the corresponding age- and sex-matched healthy control.

Abbreviations: del, deletion; Hom, homozygous; SD, standard deviation.

[1]Age is expressed in years.

[2]The term "extrarenal complications" is expressed as the number of cystinosis extrarenal manifestations present in this patient. Complications that are considered to be extrarenal manifestations of cystinosis in this score are as follows: (1) retinopathy, (2) primary hypothyroidism, (3) diabetes mellitus type 1, (4) swallowing dysfunction, and (5) distal myopathy.

significance, epidermal and papillary dermis thinning was correlated with established indicators of disease severity, including kidney function (estimated glomerular filtration rate) at the time of imaging and the average leucocyte cystine levels over a period of time before imaging, the latter being the current gold standard for therapeutic monitoring of cystinosis (Elmonem et al., 2016). Although a linear regression analysis suggested a trend toward more epidermal and papillary dermis thinning with a decline in kidney function and higher leucocyte cystine levels, no statistical significance was reached (see Supplementary Figure S3 online). Even though epidermal atrophy is present in several stages of chronic kidney disease and no control group of patients with chronic kidney disease or KTx patients was included, our data suggest that chronic kidney disease is not the only cause for the skin phenotype, which is in line with the observations of Chiavérini et al. (2013). Furthermore, in patients with cystinosis before KTx, harboring the common homozygous 57 kb deletion of *CTNS,* which abolishes all functions of cystinosin, significant thinning of the epidermis predicted the presence of extrarenal manifestations with a maximal positive predictive value (Table 1). Apart from this striking predictive value of epidermal thinning, these data suggest that similar mechanisms, which are not necessarily related solely to the transport of cystine by cystinosin, might underlie the nature of the multiorgan disease in cystinosis. Moreover, the analysis of the tissue optical characteristics of the epidermis and papillary dermis did not show to be significantly different in cystinosis. This suggests that the OCT signal originating from cystine crystal deposits is nonspecific. As a result, reflectance confocal microscopy may serve as a complementary technique for the specific identification and quantification of dermal cystine crystal deposits (Chiavérini et al., 2013). In summary, we conclude that enhanced intrinsic skin aging is a phenotypic feature of cystinosis as demonstrated by HD-OCT.

Data availability statement

Datasets related to this article can be found at https://doi.org/10.17632/jf5wtz7yg2.1 hosted at Mendeley Data (Veys and Koenraad, 2019).

ORCIDs

Koenraad R.P. Veys: http://orcid.org/0000-0002-5429-111X
Mohamed A. Elmonem: http://orcid.org/0000-0002-3154-1948
Frans Dhaenens: http://orcid.org/0000-0001-6266-6981
Maria Van Dyck: http://orcid.org/0000-0002-0605-120X
Mirian M.C.H. Janssen: http://orcid.org/0000-0003-4668-9977
Elisabeth A.M. Cornelissen: http://orcid.org/0000-0002-1156-5264
Katharina Hohenfellner: http://orcid.org/0000-0003-0978-8087
Ahmed Reda: http://orcid.org/0000-0001-7053-7979
Pascale Quatresooz: http://orcid.org/0000-0002-0140-9655
Bert van den Heuvel: http://orcid.org/0000-0003-3917-6727
Marc A.L.M. Boone: http://orcid.org/0000-0001-5326-2969
Elena Levtchenko: http://orcid.org/0000-0002-8352-7312

CONFLICT OF INTEREST

Outside of the submitted work, FD is an employee of Agfa, the manufacturer of the SkinTell device used for data collection and has not received any financial compensation; EL is an employee of Consultancy Orphan Europe and is supported by a research grant from Horizon Pharma. All other authors state no conflict of interest.

ACKNOWLEDGMENTS

On behalf of all of the authors, we would like to thank Horizon Pharma LLC for providing financial support for this study. We also explicitly would like to express our sincere appreciation and thanks to L. Deleu for her irreplaceable help in organizing the recruitment of age- and sex-matched healthy control children, adolescents, and adults. We also would like to thank all healthy controls for participating in this study, hereby offering new perspectives to the entire community of patients living with cystinosis.

EL is supported by the Research Foundation Flanders (F.W.O Vlaanderen) grant 1801110N, the Cystinosis Research Network, and Cystinosis Ireland; KRPV is funded by the Research Foundation Flanders (F.W.O Vlaanderen) grant 11Y5216N.

AUTHOR CONTRIBUTIONS

Conceptualization: KRPV, FD, MALMB, EL; Data Curation: KRPV; Formal Analysis: KRPV, MAE, FD, AR; Funding Acquisition: KRPV, MAE, FD, MVD, BvdH, EL; Investigation: KRPV, PQ, MALMB; Methodology: KRPV, FD, MALMB; Project Administration: KRPV; Resources: KRPV, MAE, FD, MVD, MMCHJ, EAMC, KH, PQ, BvdH, MALMB, EL; Software: KRPV, FD, MALMB; Supervision: BvdH, MALMB, EL; Validation: KRPV; Visualization: KRPV, PQ; Writing - Original Draft Preparation: KRPV; Writing - Review and Editing: KRPV, MAE, FD, MVD, MMCHJ, EAMC, KH, AR, BvdH, MALMB, EL

Koenraad R.P. Veys[1,2,*], Mohamed A. Elmonem[2,3], Frans Dhaenens[4], Maria Van Dyck[1], Mirian M.C.H. Janssen[5], Elisabeth A.M. Cornelissen[6], Katharina Hohenfellner[7], Ahmed Reda[2], Pascale Quatresooz[8], Bert van den Heuvel[2,6], Marc A.L.M. Boone[9] and Elena Levtchenko[1,2]

[1]Department of Pediatrics, University Hospitals Leuven, Leuven, Belgium; [2]Department of

compared with controls. Each dot represents the median of nine observations of each studied parameter per subject (cystinosis, red; control, green). Data presented as mean ± standard deviation (d) or median ± interquartile range (f). For graphical representation of (e), full straight line represents linear regression analysis of non-KTx patients with cystinosis (red line) and controls (green line). DEJ, dermal-epidermal junction; HD-OCT, high-definition optical coherence tomography; KTx, kidney transplantation; RPJ, reticular-papillary junction; SES, skin entrance signal; Str Gran, signal of the surface of the stratum granulosum.

Development & Regeneration, KU Leuven, Leuven, Belgium; [3]Department of Clinical and Chemical Pathology, Faculty of Medicine, Cairo University, Cairo, Egypt; [4]Agfa Healthcare, Mortsel, Belgium; [5]Department of Internal Medicine, Radboud University Medical Center, Nijmegen, The Netherlands; [6]Department of Pediatrics, Radboud University Medical Center, Nijmegen, The Netherlands; [7]Department of Pediatrics, SüdOstBayern Klinikum, Rosenheim, Germany; [8]Department of Pathology, Centre Hospitalier Universitaire de Liège, Liège, Belgium; and [9]Department of Dermatology, Université Libre de Bruxelles, Brussels, Belgium

[*]Corresponding author e-mail: koenraad.veys@uzleuven.be

SUPPLEMENTARY MATERIAL

Supplementary material is linked to the online version of the paper at www.jidonline.org, and at 10.1016/j.jid.2019.03.1153.

REFERENCES

Bellomo F, Signorile A, Tamma G, Ranieri M, Emma F, De Rasmo D. Impact of atypical mitochondrial cyclic-AMP level in nephropathic cystinosis. Cell Mol Life Sci 2018;75:3411–22.

Boone M, Jemec GB, Del Marmol V. High-definition optical coherence tomography enables visualization of individual cells in healthy skin: comparison to reflectance confocal microscopy. Exp Dermatol 2012;21:740–4.

Boone MA, Suppa M, Dhaenens F, Miyamoto M, Marneffe A, Jemec GB, et al. In vivo assessment of optical properties of melanocytic skin lesions and differentiation of melanoma from non-malignant lesions by high-definition optical coherence tomography. Arch Dermatol Res 2016a;308:7–20.

Boone M, Suppa M, Miyamoto M, Marneffe A, Jemec G, Del Marmol V. In vivo assessment of optical properties of basal cell carcinoma and differentiation of BCC subtypes by high-definition optical coherence tomography. Biomed Opt Express 2016b;7:2269–84.

Boone MA, Suppa M, Marneffe A, Miyamoto M, Jemec GB, Del Marmol V. High-definition optical coherence tomography intrinsic skin ageing assessment in women: a pilot study. Arch Dermatol Res 2015;307:705–20.

Cherqui S, Courtoy PJ. The renal Fanconi syndrome in cystinosis: pathogenic insights and therapeutic perspectives. Nat Rev Nephrol 2017;13:115–31.

Chiavérini C, Kang HY, Sillard L, Berard E, Niaudet P, Guest G, et al. In vivo reflectance confocal microscopy of the skin: a noninvasive means of assessing body cystine accumulation in infantile cystinosis. J Am Acad Dermatol 2013;68:e111–6.

Chiaverini C, Sillard L, Flori E, Ito S, Briganti S, Wakamatsu K, et al. Cystinosin is a melanosomal protein that regulates melanin synthesis. FASEB J 2012;26:3779–89.

Elmonem MA, Veys KR, Soliman NA, van Dyck M, van den Heuve LP, Levtchenko E. Cystinosis: a review. Orphanet J Rare Dis 2016;22:11–47.

Guillet G, Sassolas B, Fromentoux S, Gobin E, Leroy JP. Skin storage of cystine and premature skin ageing in cystinosis. Lancet 1998;352:1444–5.

Jenkins G. Molecular mechanisms of skin ageing. Mech Ageing Dev 2002;123:801–10.

Levtchenko E, de Graaf-Hess A, Wilmer M, van den Heuvel L, Monnens L, Blom H. Altered status of glutathione and its metabolites in cystinotic cells. Nephrol Dial Transplant 2005;20:1828–32.

Luciani A, Festa BP, Chen Z, Devuyst O. Defective autophagy degradation and abnormal tight junction-associated signaling drive epithelial dysfunction in cystinosis. Autophagy 2018;14:1157–9.

Moloney FJ, de Freitas D, Conlon PJ, Murphy GM. Renal transplantation, immunosuppression and the skin: an update. Photodermatol Photoimmunol Photomed 2005;21:1–8.

Schoepe S, Schäcke H, May E, Asadullah K. Glucocorticoid therapy-induced skin atrophy. Exp Dermatol 2006;15:406–20.

Where Is Itch Represented in the Brain, and How Does it Differ from Pain? An Activation Likelihood Estimation Meta-Analysis of Experimentally-Induced Itch

Journal of Investigative Dermatology (2019) **139,** 2245–2248; doi:10.1016/j.jid.2019.04.007

TO THE EDITOR

Perceptually, itch is clearly discernible from pain, yet both sensations exhibit a substantial anatomical overlap with common peripheral transmission and recruited brain regions. For example, recent functional magnetic resonance imaging (fMRI) studies have observed activations in the pain-processing network during cowhage- or histamine-induced itch in the thalamus (Leknes et al., 2007; Mochizuki et al., 2009; Papoiu et al., 2012; Valet et al., 2008), insular cortex (Herde et al., 2007; Leknes et al., 2007), cingulate cortex (Mochizuki et al., 2007), prefrontal cortex (Mochizuki et al., 2009), postcentral gyrus (Herde et al., 2007; Ishiuji et al., 2009; Papoiu et al., 2012), parietal operculum (Mochizuki et al., 2009; Papoiu et al., 2012), parahippocampal gyrus (Papoiu et al., 2012), and basal ganglia (Mochizuki et al., 2007). However, the differences in brain processing of these two types of sensation have yet to be satisfactorily determined.

The most significant advances in itch biology identifying itch-specific pathways have occurred in the peripheral nervous system, where there are itch-specific primary sensory neurons such as MrgprA3+ and NP2 (Dong and Dong, 2018). However, interneurons (GRP+) that relay itch input to the spinal cord of the central nervous system also receive pain sensory information (Sun et al., 2017). Nevertheless, there are itch-specific GRPR+ interneurons in lamina I of the spinal cord, but projection neurons to the spinothalamic tract, thalamus, and beyond are polymodal (Hachisuka et al., 2016), and thus decoding in the brain requires further exploration. To date, investigation of supraspinal processing of itch is

Abbreviations: ALE, activation likelihood estimation; fMRI, functional magnetic resonance imaging

Accepted manuscript published online 2 May 2019; corrected proof published online 27 June 2019

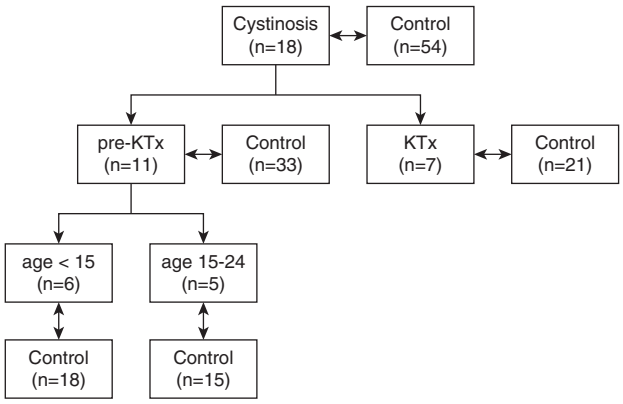

Supplementary Figure S1. Study groups and subgroups. KTx, kidney transplantation.

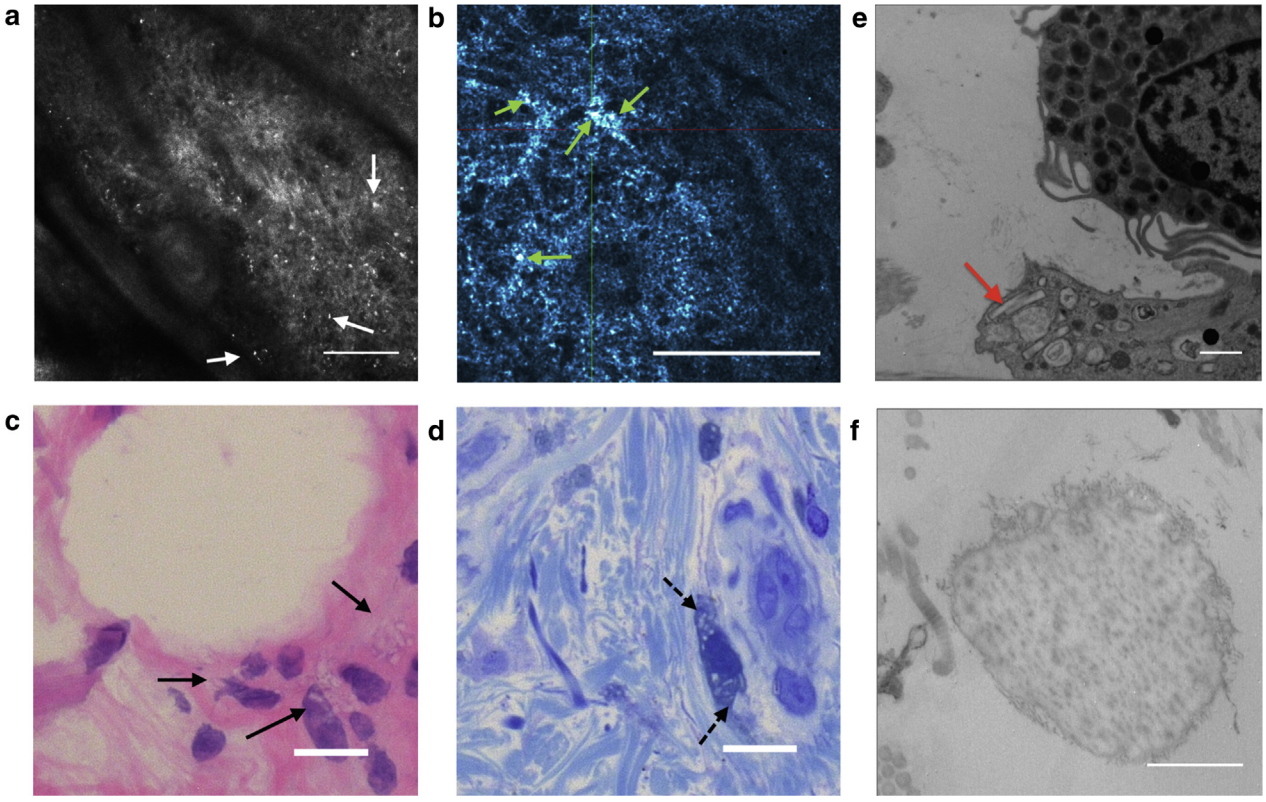

Supplementary Figure S2. Correlation of dermatological findings at the distal third of the ventral side of the upper arm in a kidney-transplanted patient with nephropathic cystinosis (patient 17) examined by RCM and HD-OCT, and its corresponding histologic and EM substrate. (**a**) RCM confocal section image of the papillary dermis showing several intense deposits corresponding to cystine crystals (white full arrows). Scale bar = 100 μm. (**b**) En-face HD-OCT image of the papillary dermis showing intense, round- to rectangular-shaped deposits surrounding the subpapillary blood vessel plexus (green arrows). Scale bar = 1,000 μm. (**c**) H&E staining on frozen punch skin biopsy tissue. Scale bar = 10 μm. Original magnification ×40. (**d**) Toluidine blue staining on glutaraldehyde fixed tissue. Numerous cystine crystal deposits surrounding the subpapillary blood vessel plexus in the reticular dermis and the vasculature in the papillary dermis (black full arrows) in proximity to histiocytes (black dashed arrows). Scale bar = 10 μm. Original magnification ×40. (**e**) EM showing cystine crystal deposits (red arrow) in dermal fibroblasts. Scale bar = 1 μm. Original magnification ×6,000. (**f**) EM showing fragmented elastin fibers with irregular contours and elastotic-like osmiophilic inclusions. Scale bar = 1 μm. Original magnification ×7,750. EM, electron microscopy; HD-OCT, high-definition optical coherence tomography; H&E, hematoxylin and eosin; RCM, reflectance confocal microscopy.

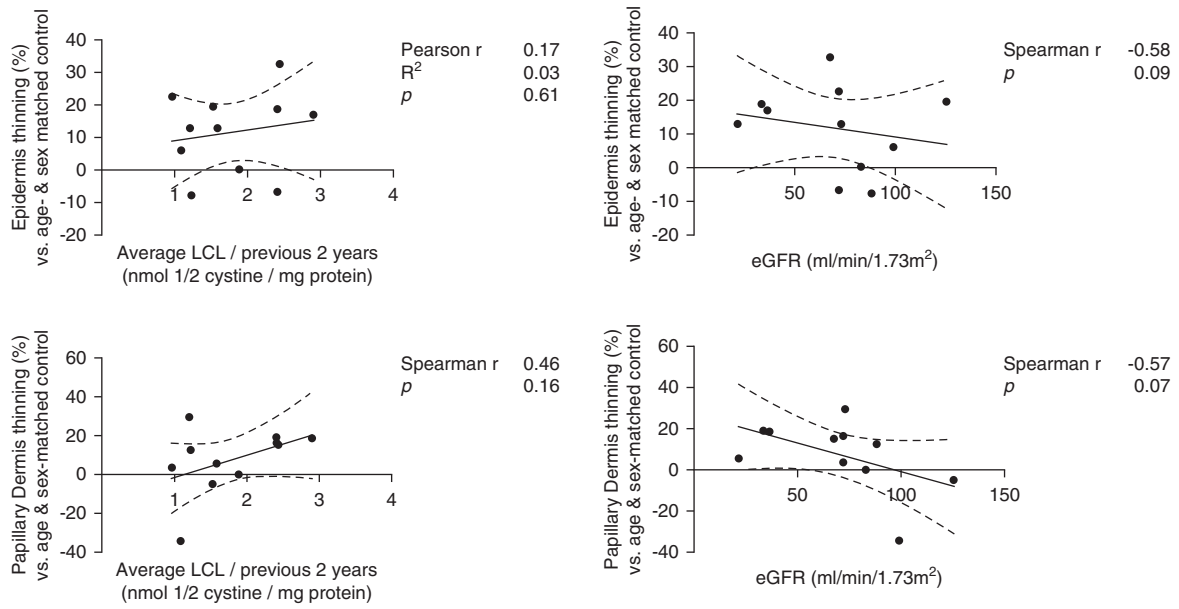

Supplementary Figure S3. Analysis of linear regression and correlation of epidermal and papillary dermis thinning versus the average leucocyte cystine level and kidney function in patients with cystinosis before kidney transplantation. eGFR, estimated glomerular filtration rate; LCL, leucocyte cystine level.

Supplementary Table S1. Clinical and Demographic Characteristics of the Cohort of Patients with Cystinosis

Patient	Sex	Age	Cystinosis Phenotype	Genetic Background	Age at Diagnosis	KTx	Age at KTx	Time Since KTx
1	M	6.4	INF	57 kb del + IVS10-7G>A	1.2	N	NA	NA
2	F	6.5	INF	Hom 57 kb del	0.9	N	NA	NA
3	M	7.6	INF	57 kb del + c.926dupG	2.4	N	NA	NA
4	F	12.1	INF	57 kb del + c.926dupG	0.8	N	NA	NA
5	M	12.5	INF	c.681G>A + c.1015G>A	0.9	N	NA	NA
6	F	14.0	JUV	57 kb del + c.198_218del21	11.3	N	NA	NA
7	F	16.0	INF	Hom 57 kb del	2.5	N	NA	NA
8	F	16.6	INF	57 kb del + c.18_21delGACT	1.3	N	NA	NA
9	M	16.9	INF	Hom 57 kb del	0.8	N	NA	NA
10	M	18.0	INF	Hom 57 kb del	0.9	N	NA	NA
11	M	22.2	INF	Hom 57 kb del	1.0	N	NA	NA
12	M	24.6	INF	Hom c.926dupG	1.0	Y	8.9	15.7
13	F	25.6	INF	Hom 57 kb del	1.7	Y	9.4	16.2
14	M	29.5	INF	57 kb del + c.1015G>A	1.0	Y	20	9.6
15	F	30.6	INF	57 kb del + c.141-24T>C	3.4	Y	12.9	17.7
16	F	34.0	INF	Hom 57 kb del	1.2	Y	12.3	21.7
17	M	38.0	INF	Hom 57 kb del	2.4	Y	14.0	24.1
18	F	42.2	INF	57 kb del + c.926dupG	2.0	Y	11.6	—
—	—	—	—	—	—	—	12.3	29.9

Abbreviations: del, deletion; F, female; Hom, homozygous; INF, infantile nephropathic cystinosis; JUV, juvenile nephropathic cystinosis; KTx, kidney transplantation; M, male; N, no; NA, not applicable; Y, yes.

Supplementary Table S2. Established Hallmarks in the OCT Signal Versus Image Depth Plot of an HD-OCT Image and their Corresponding Anatomical Substrates[1]

Abbreviation	Full Description	Definition
SES	Skin entrance signal	First peak of the OCT signal versus image depth plot.
Str. Gran.	Signal of the surface of the stratum granulosum	The first intense signal below the stratum corneum in an HD-OCT skin image, corresponding to the second peak of the OCT signal versus image depth plot.
DEJ	Dermal-epidermal junction	The first valley in the OCT signal versus image depth plot, following the skin entrance signal.
RPJ	Reticular-papillary junction	The highest peak in the OCT signal versus image depth plot, following the dermal-epidermal junction.

Abbreviation: HD-OCT, high-definition optical coherence tomography.
[1]Boone et al., 2012; Boone et al., 2015; Boone et al., 2016a; Boone et al., 2016b.

Supplementary Table S3. Parameters Yielded by the Analysis of the OCT Signal Versus Image Depth Plot Acquired from an HD-OCT Skin Image Following Assignment of the Established Hallmarks

Abbreviation	Full Description	Definition	Unit
ET	Epidermal thickness (viable epidermis)	Distance between the second peak and the first valley of the OCT signal versus image depth plot.	µm
PDT	Papillary dermis thickness	Distance between the first valley and the highest peak after the valley of the OCT signal versus image depth plot.	µm
I_{SES}	Intensity of the OCT signal at the skin entrance	Intensity (magnitude) of the OCT signal at the first peak of the OCT signal versus image depth plot, corresponding to the surface of the stratum corneum, expressed in AU.	AU
$I_{Str\ Gran}$	Intensity of the OCT signal at the surface of the stratum granulosum	Intensity (magnitude) of the OCT signal at the second peak of the OCT signal versus image depth plot, corresponding to the surface of the stratum granulosum, expressed in AU.	AU
I_{DEJ}	Intensity of the OCT signal at the dermal-epidermal junction	Intensity (magnitude) of the OCT signal at the first valley of the OCT signal versus image depth plot, corresponding to the DEJ, expressed in AU.	AU
I_{RPJ}	Intensity of the OCT signal at the reticular-papillary junction	Intensity (magnitude) of the OCT signal at the highest peak after the valley of the OCT signal versus image depth plot, corresponding to the RPJ, expressed in AU.	AU
$I_{DEJ}/I_{Str\ Gran}$	Intensity of the DEJ normalized to the intensity of the surface of the stratum granulosum		AU
$I_{RPJ}/I_{Str\ Gran}$	Intensity of the RPJ normalized to the intensity of the surface of the stratum granulosum		AU
μ_{raf} Epidermis	Relative attenuation factor of the (viable) epidermis	Direction coefficient of the slope of the log-transformed curve of the (viable) epidermis section of OCT signal versus image depth plot. Corresponds to the reduced scattering coefficient, indicating the number of scattering events per unit of distance.	μm^{-1}
μ_{raf} PD	Relative attenuation factor of the papillary dermis	Direction coefficient of the slope of the log-transformed curve of the papillary dermis section of OCT signal versus image depth plot. Corresponds to the reduced scattering coefficient, indicating the number of scattering events per unit of distance.	μm^{-1}

Abbreviations: AU, arbitrary units; DEJ, dermal-epidermal junction; HD-OCT, high-definition optical coherence tomography; RPJ, reticular-papillary junction.

Supplementary Table S4. Validation of Our Methodology of HD-OCT Image Analysis Based on the Assessment of the OCT Signal Versus Image Depth Plot

HD-OCT Parameter	Young-Aged Controls	Medium-Aged Controls	*P*-Value
N	33	21	—
Age (years), mean ± SEM	13.4 ± 0.9	32.4 ± 1.2	—
F:M ratio	15:18	12:9	—
Thickness			
Epidermis (μm), mean ± SEM	86.3 ± 2.0	73.7 ± 3.0	0.0008[2]
Papillary dermis (μm), mean ± SEM	65.9 ± 1.7	57.1 ± 3.5	0.015[1]
OCT signal intensity			
$I_{Str\ Gran}$ (AU), mean ± SEM	440.9 ± 10.5	466.6 ± 13.9	0.142
I_{DEJ} (AU), mean ± SEM	71.53 ± 2.6	89.9 ± 3.1	<0.0001[2]
I_{RPJ} (AU), mean ± SEM	162.7 ± 6.0	181.5 ± 7.8	0.060
$I_{DEJ}/I_{Str\ Gran}$ (AU), median (p25; p75)	0.17 (0.14; 0.18)	0.19 (0.18; 0.21)	0.0001[2]
$I_{RPJ}/I_{Str\ Gran}$ (AU), median (p25; p75)	0.39 (0.31; 0.43)	0.38 (0.33; 0.42)	0.986
Attenuation			
μ_{raf} Epidermis (μm^{-1}), mean ± SEM	0,020 ± 0.0003	0.021 ± 0.0006	0.131
μ_{raf} Papillary dermis (μm^{-1}), median (p25; p75)	−0.010 (−0.013; −0.009)	−0.011 (−0.014; −0.007)	0.954

A highly significant reduction in epidermal thickness, a significant reduction in papillary dermis thickness, and an increase of the intensity of the OCT signal at the DEJ (including the I_{DEJ} normalized to $I_{Str\ Gran}$, $I_{DEJ}/I_{Str\ Gran}$) is demonstrated in young-aged (<24 years) versus medium-aged (24−40 years) healthy control subjects. These findings are in line with the observations of Boone et al. (2015), validating our methodology of HD-OCT image analysis, and the use of these parameters for the objectives in this study.

Abbreviations: AU, arbitrary units; DEJ, dermal-epidermal junction; F, female; HD-OCT, high-definition optical coherence tomography; I, intensity; M, male; RPJ, reticular-papillary junction; SEM, standard error of the mean; Str Gran, stratum granulosum; μ_{raf}, relative attenuation factor.

[1] $P \leq 0.05$.

[2] $P \leq 0.001$.

Supplementary Table S5. Thickness and the Tissue Optical Characteristics of Epidermis and Papillary Dermis as Assessed by HD-OCT in Patients with Cystinosis Versus Age- and Sex-Matched Controls

HD-OCT Parameter	Cystinosis	Control	*P*-Value
N	18	54	—
Age (years), mean ± SEM	20.7 ± 2.5	20.8 ± 1.5	—
F:M ratio	9:9	27:27	—
Thickness			
Epidermis (μm), mean ± SEM	71.4 ± 2.7	81.4 ± 1.9	0.007[1]
Papillary dermis (μm), mean ± SEM	51.5 ± 3.9	62.3 ± 1.8	0.006[1]
OCT signal intensity			
$I_{Str\ Gran}$ (AU), mean ± SEM	432.6 ± 14.7	450.9 ± 8.5	0.284
I_{DEJ} (AU), median (p25; p75)	79.0 (68.5; 89.1)	79.9 (68.9; 90.7)	0.854
I_{RPJ} (AU), mean ± SEM	160.5 ± 9.4	170 ± 4.9	0.346
$I_{DEJ}/I_{Str\ Gran}$ (AU), median (p25; p75)	0.20 (0.17; 0.21)	0.18 (0.16; 0.20)	0.050
$I_{RPJ}/I_{Str\ Gran}$ (AU), median (p25; p75)	0.35 (0.30; 0.42)	0.39 (0.32; 0.43)	0.242
Attenuation			
μ_{raf} Epidermis (μm^{-1}), median (p25; p75)	0.02 (0.020; 0.023)	0.02 (0.019; 0.021)	0.108
μ_{raf} Papillary dermis (μm^{-1}), median (p25; p75)	−0.01 (−0.014; −0.007)	−0.01 (−0.013; −0.008)	0.678

Abbreviations: AU, arbitrary units; DEJ, dermal-epidermal junction; F, female; HD-OCT, high-definition optical coherence tomography; *I*, intensity; M, male; RPJ, reticular-papillary junction; SEM, standard error of the mean; Str Gran, stratum granulosum; μ_{raf}, relative attenuation factor.

[1] $P \leq 0.01$.

Supplementary Table S6. Epidermal and Papillary Dermis Thickness in the Subgroup of Adolescent and Young Adult Patients with Cystinosis (Aged 15–24 Years) Before Kidney Transplantation Versus Age- and Sex-Matched Controls

HD-OCT Parameter	Adolescent Cystinosis Patient Before KTx	Control	*P*-Value
N	5	15	—
Age (years), mean ± SEM	17.9 ± 1.1	17.8 ± 0.7	—
F:M ratio	2:3	6:9	—
Thickness			
Epidermis (µm), median (p25; p75)	68.6 (66.4; 74.2)	81.9 (73.1; 97.4)	0.010[1]
Papillary dermis (µm), median (p25; p75)	56.5 (50.9; 57.6)	65.3 (56.5; 74.2)	0.031[1]

Abbreviations: F, female; KTx, kidney transplantation; M, male; SEM, standard error of the mean.
[1] $P \leq 0.05$.